PERGAMON

International Journal of Heat and Mass Transfer 44 (2001) 575–586

International Journal of HEAT and MASS TRANSFER

www.elsevier.com/locate/ijhmt

A hybrid spatial differencing scheme for discrete ordinates method in 2D rectangular enclosures

Il-Kyoung Kim[a], Woo-Seung Kim[b,*]

[a]*Department of Mechanical Engineering, Hanyang University, 17 Haengdang-dong, Seongdong-ku, Seoul 133-791, South Korea*
[b]*Department of Mechanical Engineering, Hanyang University, 1271 Sa 1-dong, Ansan-si, Kyonggi-do 425-791, South Korea*

Received 15 July 1999; received in revised form 15 March 2000

Abstract

A hybrid spatial differencing scheme for the discrete ordinates method is proposed to predict radiation intensity in a two-dimensional rectangular enclosure. Since the hybrid scheme incorporates the strengths from the diamond scheme and the step scheme, and takes into consideration the characteristics of the medium, it is more accurate and yields more stable results. Several other spatial differencing schemes are examined to address the effect of numerical smearing (or false scattering). Predictions from the present hybrid scheme are compared to those of the other schemes for transparent, purely absorbing, purely scattering, and absorbing–emitting–isotropically scattering media. It is found that the proposed scheme predicts more stable and less smeared results than the others.

1. Introduction

Discrete Ordinates Method (DOM) has received the main consideration for the analysis of radiative heat transfer [1–3]. DOM is the method that approximates Radiative Transport Equation (RTE), which is integro-differential equation, to first order differential equation. Its algorithm is simple and it is easy to apply it to typical Finite Volume Method (FVM) [4]. However, there are some problems that must be addressed in the application of DOM. The ray effect may occur due to the approximation of continuously distributed ray to discrete ordinates, and false scattering [5] (or numerical smearing [6]) may result from the disagreement of directions between grid and ordinate.

Many researchers have studied the modification of DOM to overcome these defects. Raithby and Chui [7] and Kim and Baek [8] proposed FVM and modified DOM, respectively. Pessoa-Filho and Thynell [9] employed an analytical method and Mohamad [10] proposed the use of Local Analytical DOM (LADOM). Cheong and Song [11] used second order DOM for compatibility with typical transport equations.

False scattering occurring in multi-dimensional problems cannot be excluded completely from DOM, but it can be minimized by using a proper spatial differencing scheme [12]. Among the spatial differencing schemes the step and the diamond/central differencing schemes have been used most often. Since these schemes are not accurate and not stable, the positive [13–15] and the variable-weight schemes [16,17] were developed to overcome these shortcomings. These schemes use the fix-up procedure to assist the diamond scheme to predict physically appropriate solution. The

* Corresponding author. Tel.: +82-345-400-5248; fax: +82-345-406-5550.
E-mail address: wskim@email.hanyang.ac.kr (W.-S. Kim).

0017-9310/01/$ - see front matter
PII: S0017-9310(00)00114-9

Nomenclature

E_b	emissive power, πI_b	Δx, Δy	dimensions of a control volume
f	spatial differencing weight	Φ	scattering phase function
G	incident radiation	κ	absorption coefficient
I	radiation intensity	σ_s	scattering coefficient
I_b	black body intensity	μ, ξ	directional cosine
L_x, L_y	dimensions of a rectangular enclosure	Ω	solid angle
N	total number of ordinates		
S	source term in Eq. (2b)	*Superscripts and subscripts*	
s	radiation direction	$'$	incident direction
s	distance along a beam in a direction **s**	m	ordinate index
w	angular weight	E, W, N, S	labels for nodes within control volume
x, y	Cartesian coordinate	e, w, n, s	labels for interfaces between control volumes
Greek symbols		H	hybrid spatial differencing scheme
β	extinction coefficient, $\beta = \kappa + \sigma_s$	P	nodal point

various spatial differencing schemes such as exponential and higher-order schemes have been recently developed. However, these schemes also need the fix-up procedure and their computational procedure is not simple. Chai et al. [12] presented the characteristics of various spatial differencing schemes, and Jessee and Fiveland [6] introduced the bounded High Resolution (HR) scheme.

In the present work, a new hybrid spatial differencing scheme has been developed to obtain an accurate and stable solution to RTE. The present hybrid scheme minimizes numerical smearing of DOM in 2D rectangular enclosure and does not require the fix-up procedure by excluding the appearance of physically unrealistic radiation intensity. It has been applied to four different media: transparent, absorbing, scattering, and absorbing–emitting–isotropically scattering media. These results are compared to those of other spatial differencing schemes.

2. Governing equation

The radiative transport equation for 2D Cartesian coordinates is as follows:

$$\mu\frac{\partial I}{\partial x}+\xi\frac{\partial I}{\partial y}=-\beta I+\kappa I_b+\frac{\sigma_s}{4\pi}\int_{\Omega'=4\pi} I(\Omega')\Phi(\Omega'\to\Omega)\,d\Omega' \quad (1)$$

The following discrete ordinates equation can be obtained by applying DOM to Eq. (1).

$$\mu_m\frac{\partial I^m}{\partial x}+\xi_m\frac{\partial I^m}{\partial y}=-\beta I^m+S^m \quad (2a)$$

where

$$S^m=\kappa^m I_b+\frac{\sigma_s}{4\pi}\sum_{m'=1}^{N} w_m\Phi^{m'm}I^{m'} \quad (2b)$$

Integrating Eq. (2) over a control volume shown in Fig. 1 gives

$$\mu_m\Delta y\left(I_e^m-I_w^m\right)+\xi_m\Delta x\left(I_n^m-I_s^m\right)=\left(-\beta_P I_P^m+S_P^m\right)\Delta x\Delta y \quad (3)$$

The final discretized equation for nodal point P can be obtained by applying spatial differencing equation to Eq. (3). For $\mu_m > 0$, $\xi_m > 0$ directions, spatial differencing equation and discrete ordinates equation are as follows:

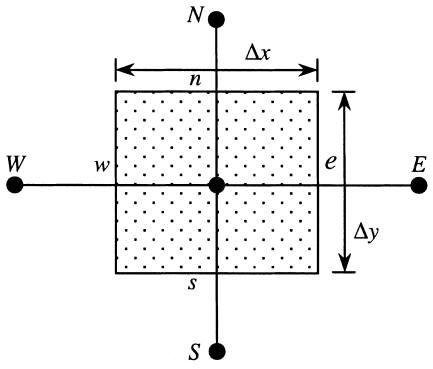

Fig. 1. Typical internal control volume.

$$I_{\mathrm{P}}^m = \left(1 - f_x^m\right) I_{\mathrm{w}}^m + f_x^m I_{\mathrm{e}}^m = \left(1 - f_{\mathrm{y}}^m\right) I_{\mathrm{s}}^m + f_{\mathrm{y}}^m I_{\mathrm{n}}^m \tag{4}$$

$$I_{\mathrm{P}}^m = \frac{\dfrac{\mu_m \Delta y}{f_x^m} I_{\mathrm{w}}^m + \dfrac{\xi_m \Delta x}{f_y^m} I_{\mathrm{s}}^m + S_{\mathrm{P}}^m \Delta x \Delta y}{\dfrac{\mu_m \Delta y}{f_x^m} + \dfrac{\xi_m \Delta x}{f_y^m} + \beta_{\mathrm{P}} \Delta x \Delta y} \tag{5}$$

where f_x^m and f_y^m are spatial differencing weights to the x and y directions, respectively.

For $\mu_m > 0$, $\xi_m > 0$ directions, Eq. (5) gives the radiation intensity at nodal point P and downstream intensities I_{e}^m and I_{n}^m can be obtained from Eq. (4).

In general, spatial differencing weights used in the step and diamond differences are $f = f_x^m = f_y^m = 1.0$ and $f = f_x^m = f_y^m = 0.5$, respectively. It is known from the numerical consideration that diamond difference is more accurate than step difference, but diamond difference sometimes produces unrealistic under-shooting (including the occurrence of negative intensity) and/or over-shooting whereas step difference is always physically stable.

To prevent these shortcomings in the diamond scheme, Lathrop and Carlson [15] proposed the negative intensity fix-up procedure that sets the negative intensity to zero, and Lathrop [13] proposed the positive scheme that always ensures positive intensity. But they did not consider the appearance of over-shooting. Jamaluddin and Smith [16] and Sanchez and Smith [17] used the variable-weight scheme that increases the spatial differencing weight f from 0.5 to 1.0 until the proper intensities are encountered. But this requires additional iteration and more computational time to predict proper intensities. Also, it needs physically strict limits of intensity to increase the confidence of computed results.

3. Analysis

3.1. A hybrid spatial differencing scheme

For convenience, only the positive directions are considered in the hybrid spatial differencing scheme.

The discrete ordinates equation given by Eq. (5) can be rewritten as follows:

$$I_{\mathrm{P}}^m = \frac{\dfrac{\mu_m \Delta y}{f_x^m} I_{\mathrm{w}}^m + \dfrac{\xi_m \Delta x}{f_y^m} I_{\mathrm{s}}^m}{\dfrac{\mu_m \Delta y}{f_x^m} + \dfrac{\xi_m \Delta x}{f_y^m} + A} + B \tag{6a}$$

where

$$A = \beta_{\mathrm{P}} \Delta x \Delta y \geq 0 \tag{6b}$$

$$B = \frac{S_{\mathrm{P}}^m \Delta x \Delta y}{\dfrac{\mu_m \Delta y}{f_x^m} + \dfrac{\xi_m \Delta x}{f_y^m} + \beta_{\mathrm{P}} \Delta x \Delta y} \geq 0 \tag{6c}$$

Following conditions can be obtained from the consideration of physical situation.

CASE I Non-participating media

$$0 \leq I_{\mathrm{P}}^m \leq \max\left[I_{\mathrm{w}}^m, I_{\mathrm{s}}^m\right] \quad \text{for} \quad A = 0, B = 0 \tag{7a}$$

CASE II Purely absorbing media

$$0 \leq I_{\mathrm{P}}^m < \max\left[I_{\mathrm{w}}^m, I_{\mathrm{s}}^m\right] \quad \text{for} \quad A > 0, B = 0 \tag{7b}$$

CASE III Absorbing, emitting and/or scattering media

$$B \leq I_{\mathrm{P}}^m < \max\left[I_{\mathrm{w}}^m, I_{\mathrm{s}}^m\right] + B \quad \text{for} \quad A > 0, B > 0 \tag{7c}$$

If I_{P}^m satisfies CASES I and II, then it also satisfies CASE III.

For a non-participating medium (CASE I), the step and the diamond schemes show the aforementioned problems, but they have the characteristics of predicting the exact solutions to special directions.

Consider a rectangular enclosure with black walls, containing a non-participating medium as shown in Fig. 2(a). When the marked part ($0.25 \leq x \leq 0.5$, $y = 0$) of the lower wall only emits a unit black body intensity ($I_{\mathrm{b}} = 1$), the distributions of radiation intensity from step and diamond schemes for a special direction are depicted in Fig. 2(b) and (c), respectively. It is shown that the step and the diamond schemes predict exact solutions for the directions of the edge and the diagonal of control volume, respectively.

A hybrid spatial differencing scheme for a non-participating medium is constructed to use these characteristics of the step and diamond schemes as follows:

$$f_{\mathrm{H,\,trans}}^m = f_x^m = f_y^m = \frac{1}{1 + \gamma^m} \tag{8a}$$

where

$$\gamma^m = \begin{cases} \dfrac{\Delta y}{\Delta x}\left|\dfrac{\mu_m}{\xi_m}\right|, & \Delta y|\mu_m| < \Delta x|\xi_m| \\ \dfrac{\Delta x}{\Delta y}\left|\dfrac{\xi_m}{\mu_m}\right|, & \Delta y|\mu_m| \geq \Delta x|\xi_m| \end{cases} \tag{8b}$$

The hybrid spatial differencing weight $f_{\mathrm{H,\,trans}}^m$ for a

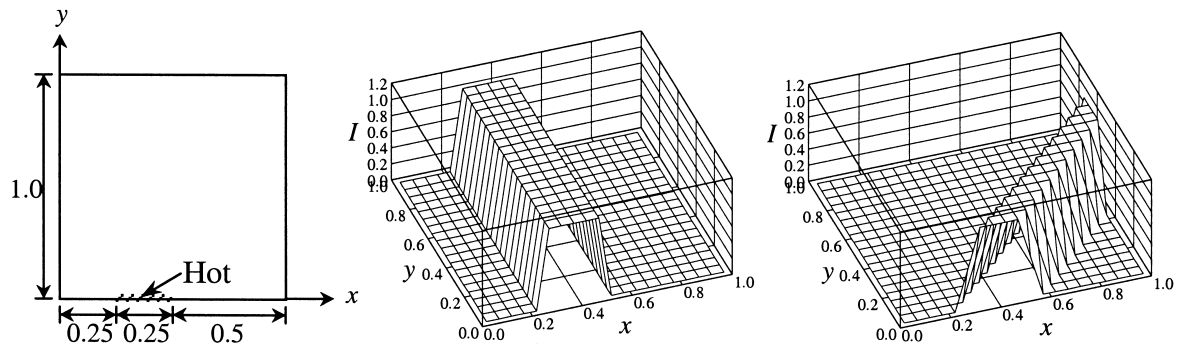

Fig. 2. Intensity distribution in a special direction ($\Delta x = \Delta y$): (a) schematic of test problem; (b) step scheme for $\mu_m = 0$, $\xi_m = 1$; (c) diamond scheme for $\mu_m = \xi_m = 1/\sqrt{2}$.

non-participating medium, being a function of the geometry of grid and the direction of ordinate, has a value between 0.5 and 1.0. For the directions of edge and diagonal of control volume, it has the values of 1.0 and 0.5, and each value corresponds to the step and the diamond schemes, respectively.

Like previously derived for a transparent medium (CASE I), there also exists a spatial differencing weight that can predict the exact solution for a special direction in an absorbing medium (CASE II).

The RTE and the exact solution for an absorbing medium is given as:

$$\frac{\mathrm{d}I}{\mathrm{d}s} + \kappa I = 0 \tag{9}$$

$$I = I_{\mathrm{u}} \mathrm{e}^{-\kappa s} \tag{10}$$

where I_{u} and s represent the upstream value of the intensity and distance along a beam in a direction **s**,

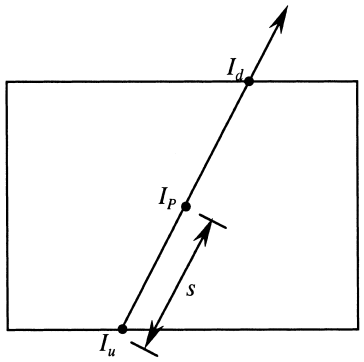

Fig. 3. Control volume and the direction of radiative transport.

respectively. These relations can be applied to a typical control volume shown in Fig. 3.

The nodal point value I_{P} and downstream value I_{d} can be derived from Eqs. (4) and (10) as follows:

$$I_{\mathrm{P}} = \left(1 - f_{\mathrm{H,\ absorb}}\right) I_{\mathrm{u}} + f_{\mathrm{H,\ absorb}} I_{\mathrm{d}} \tag{11}$$

$$I_{\mathrm{P}} = I_{\mathrm{u}} \mathrm{e}^{-\kappa s} \tag{12a}$$

$$I_{\mathrm{d}} = I_{\mathrm{u}} \mathrm{e}^{-\kappa(2s)} \tag{12b}$$

Substituting Eq. (12) into Eq. (11), the hybrid spatial differencing weight for an absorbing medium is given by

$$f_{\mathrm{H,\ absorb}} = \frac{1}{1 + \mathrm{e}^{-\kappa s}} \tag{13}$$

Here, $f_{\mathrm{H,\ absorb}}$ represents spatial differencing weight for an exact solution when positions of I_{u} and I_{d} coincide with the positions of I_{e}^m, I_{w}^m, I_{n}^m, and I_{s}^m. That is, the exact solution can be obtained when the direction of the ordinate coincides with the direction of the grid.

γ^m and $\mathrm{e}^{-\kappa s}$ in the denominators of Eqs. (8) and (13) represent the relation between the grid and the ordinate, and the characteristics of medium, respectively, and they have values between 0 and 1. For the medium which satisfies Eq. (2) and has the characteristics of two weights, $f_{\mathrm{H,\ trans}}^m$ and $f_{\mathrm{H,\ absorb}}$, the spatial differencing weight, f_{H}^m, can be defined as:

$$f_{\mathrm{H}}^m = f_x^m = f_y^m = \min\left[\frac{1}{\gamma^m + \mathrm{e}^{-\beta s^m}}, 1\right] \tag{14a}$$

where γ^m is given by Eq. (8b) and the distance along a beam in a direction **s**, s^m, is defined as follows:

$$s^m = \begin{cases} \dfrac{\Delta y}{2|\xi_m|}, & \Delta y|\mu_m| < \Delta x|\xi_m| \\ \dfrac{\Delta x}{2|\mu_m|}, & \Delta y|\mu_m| \geq \Delta x|\xi_m| \end{cases} \tag{14b}$$

The following three cases have been solved to examine if f_{H}^m, given by Eq. (14a), is stable and applicable to non-participating, absorbing, and absorbing–emitting–scattering media, respectively.

Chai et al. [12] showed analytically that for $\mu_m > 0$, $\xi_m > 0$ directions, with $I_{\mathrm{w}}^m = 0$ and $\Delta x = \Delta y$ in the purely absorbing medium, the step scheme predicts physically realistic solution, but the diamond scheme predicts the negative value of I_{n}^m for $\mu_m \geq \xi_m$. The hybrid scheme considered in this study is applied to the case of Chai et al. and the following results are obtained.

For $\mu_m \geq \xi_m$, the following two relations are obtained by combining Eqs. (4), (5), and (14):

$$I_{\mathrm{P}}^m = \frac{\left(\mu_m \mathrm{e}^{-\beta s^m} + \xi_m\right)\xi_m I_{\mathrm{s}}^m + S^m \Delta y \mu_m}{\left(\mu_m \mathrm{e}^{-\beta s^m} + \xi_m\right)\left(\mu_m + \xi_m\right) + \beta \Delta y \mu_m} \tag{15}$$

$$I_{\mathrm{n}}^m = \frac{\mu_m \mathrm{e}^{-\beta s^m} + \xi_m}{\mu_m}\left(I_{\mathrm{P}}^m - \frac{\mu_m \mathrm{e}^{-\beta s^m} + \xi_m - \mu_m}{\mu_m \mathrm{e}^{-\beta s^m} + \xi_m} I_{\mathrm{s}}^m\right) \tag{16}$$

The condition for $I_n^m \geq 0$ in Eq. (16) is given by:

$$(1 - \mathrm{e}^{-\beta s^m}) I_{\mathrm{s}}^m \geq \frac{\beta \Delta y}{\mu_m}\left(\frac{\mu_m \mathrm{e}^{-\beta s^m} + \xi_m - \mu_m}{\mu_m \mathrm{e}^{-\beta s^m} + \xi_m} I_{\mathrm{s}}^m - \frac{S^m}{\beta}\right) \tag{17}$$

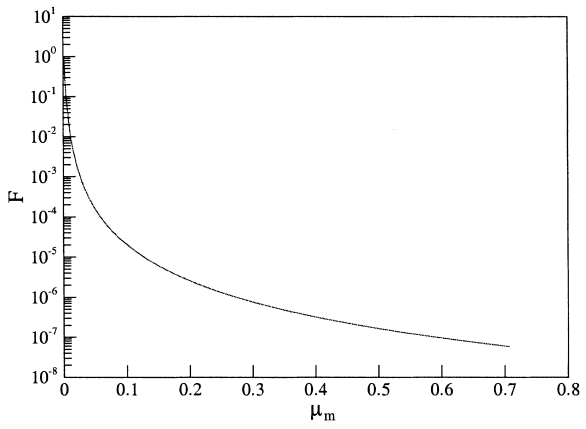

Fig. 4. Distribution of F due to the change of μ_m.

For the purely absorbing medium ($S^m = 0$, $\beta = \kappa$), Eq. (17) has more severe condition than for the absorbing–emitting–scattering medium ($S^m \geq 0$). The condition for $I_n^m \geq 0$ in the purely absorbing medium becomes

$$F = (1 - \mathrm{e}^{-\kappa s^m}) - \frac{\kappa \Delta y}{\mu_m}\frac{\mu_m \mathrm{e}^{-\kappa s^m} + \xi_m - \mu_m}{\mu_m \mathrm{e}^{-\kappa s^m} + \xi_m} \geq 0 \tag{18}$$

F automatically satisfies the condition given by Eq. (18), irrespective of the values of μ_m, ξ_m, κ, and Δy. The distribution of F for a special case ($\kappa = 1.0$, $\Delta y = 0.01$, $\mu_m = \xi_m$) is depicted in Fig. 4.

For $\mu_m < \xi_m$, the condition $I_n^m \geq 0$ is always satisfied in the same manner for $\mu_m \geq \xi_m$. The radiation intensity of the right face of the control volume, I_{e}^m, is given by Eq. (19) and always has a positive value.

$$I_{\mathrm{e}}^m = \frac{\mu_m \mathrm{e}^{-\kappa s^m} + \xi_m}{\mu_m} I_{\mathrm{P}}^m \tag{19}$$

3.2. Spatial differencing scheme and numerical smearing

Fig. 5 shows the distributions of the radiation intensity for arbitrary direction from several spatial differencing schemes when there exists a non-participating medium in the enclosure shown in Fig. 2(a). Whereas smearing and under-/over-shooting appear in the step and the diamond schemes, respectively, it can be seen that the hybrid scheme predicts more accurate results and does not show the under-/over-shooting. Not included in this figure, Lathrop's positive scheme [13] defined in Eq. (20) predicts the same results as the hybrid scheme.

$$f_x^m = \max\left[1 - D_y^m / D_x^m \left(D_y^m + 2\right), 0.5\right] \tag{20a}$$

$$f_y^m = \max\left[1 - D_x^m / D_y^m \left(D_x^m + 2\right), 0.5\right] \tag{20b}$$

where

$$D_x^m = \frac{\beta \Delta x}{|\mu_m|} \tag{20c}$$

$$D_y^m = \frac{\beta \Delta y}{|\xi_m|} \tag{20d}$$

The modified-exponential scheme of Chai et al. [18] given by Eq. (21) becomes identical to the step scheme for a non-participating medium ($\beta = 0$).

$$I_{\mathrm{e}}^m = I_{\mathrm{P}}^m \mathrm{e}^{-\beta d_{\mathrm{e}}^m} + \left(\frac{S^m}{\beta}\right)_{\mathrm{P}} (1 - \mathrm{e}^{-\beta d_{\mathrm{e}}^m}) \tag{21a}$$

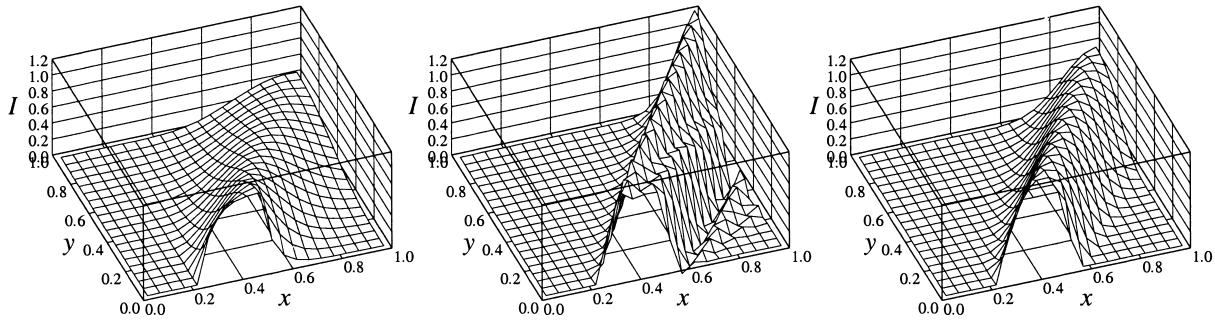

Fig. 5. Intensity distribution for non-participating medium in an arbitrary direction ($\mu_m = 0.52250$, $\xi_m = 0.85264$): (a) step scheme; (b) diamond scheme; (c) hybrid scheme.

$$I_{\mathrm{n}}^m = I_{\mathrm{P}}^m \mathrm{e}^{-\beta d_{\mathrm{n}}^m} + \left(\frac{S^m}{\beta}\right)_{\mathrm{P}} (1 - \mathrm{e}^{-\beta d_{\mathrm{n}}^m}) \tag{21b}$$

where d_{e}^m and d_{n}^m represent the distance from an arbitrary point to the center point of east and north faces of control volume, respectively, according to the direction of ordinate.

When a square enclosure with one hot ($I_{\mathrm{b}} = 1$, $y = 0$) and three cold black walls is filled with purely absorbing medium with absorption coefficient of unity, the intensity distributions from the hybrid scheme are shown in Fig. 6. It is shown that there is little numerical smearing in the direction of the diagonal of control volume. It is similar to the one in a non-participating medium and it also indicates that the smaller the grid size becomes, the closer the results get to the exact solution.

Fig. 7 shows the intensity distributions from various schemes for the particular grid ($2\Delta x = \Delta y$) and direction ($\mu_m = 0.47925$, $\xi_m = 0.87768$) in the enclosure considered above. Similar to the case of a non-participating medium, the step scheme (a) shows strong numerical smearing, but the positive scheme (b) with steep intensity distribution exhibits weak numerical smearing. However, the positive scheme yields physically unrealistic results with negative intensities. Hence, it needs the fix-up procedure. It is also shown that the modified-exponential scheme (c) exhibits strong numerical smearing like the step scheme. But its intensity distribution near the hot wall seems to be predicted more properly than that of the step scheme, because the exponential-based spatial differencing scheme represents the absorption characteristics of the medium more precisely. It is shown that the hybrid scheme (d) predicts less smeared results than the step and modified-exponential schemes and presents physically realistic results. Comparing the intensity distributions of Figs. 6(b) and 7(d), it is observed that there appears little numerical smearing in a diagonal direction of grid, but there exists smearing in other directions. This results from the fact that it is impossible to completely eliminate numerical smearing in all directions except the diagonal direction due to the characteristics of the rectangular grid.

Shown in Fig. 8 are intensity distributions for a special direction ($\mu_m = 0.8040087$, $\xi_m = 0.5773503$)

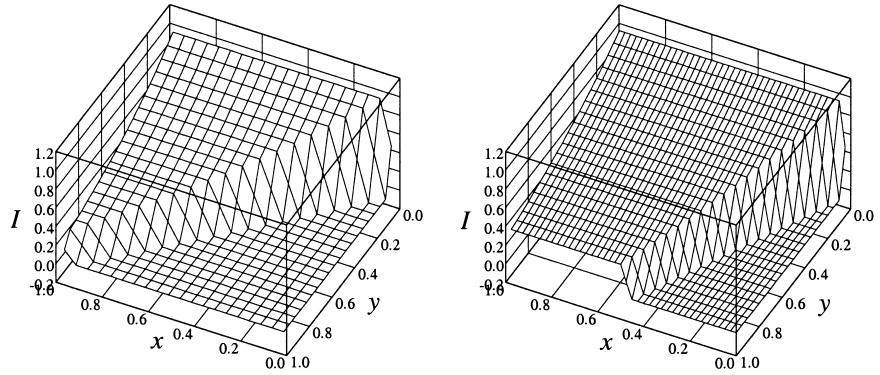

Fig. 6. Intensity distribution of hybrid scheme for purely absorbing medium: (a) $\Delta x = \Delta y$, $\mu_m = \xi_m$; (b) $2\Delta x = \Delta y$, $\mu_m = 2\xi_m$.

when the square enclosure is filled with purely absorbing medium ($\kappa = 1$) of unit emissive power ($E_b = 1$). It is shown that bounded HR: CLAM (c) of Jessee and Fiveland [6] and the hybrid scheme (d) predict results closer to the exact solution (a) than the step scheme (b).

4. Applications

4.1. Surface radiation in a rectangular enclosure

For an analysis of surface radiation in a 2D rectangular enclosure the model considered by Sanchez and Smith [17] has been used. As shown in Fig. 9, the enclosure consists of one left black wall and three black walls with temperatures of 310 and 300 K, respectively.

In Fig. 9, the dimensionless wall distance (ζ) has its origin at the lower left-hand corner of the west wall and extends clockwise around the enclosure. An ordinates set with equal angular weights and angular increment was used, and M represents the number of ordinates per quadrant.

The local heat flux distributions at the surface for $\zeta = 2.0$–2.5 (the surface from the upper right-hand corner to the center of the right wall) are depicted in Fig. 10 using a 60×60 grid system. It can be seen that the local heat flux distribution oscillates when M is 10, 15, and 25, but the amplitude of oscillation decreases

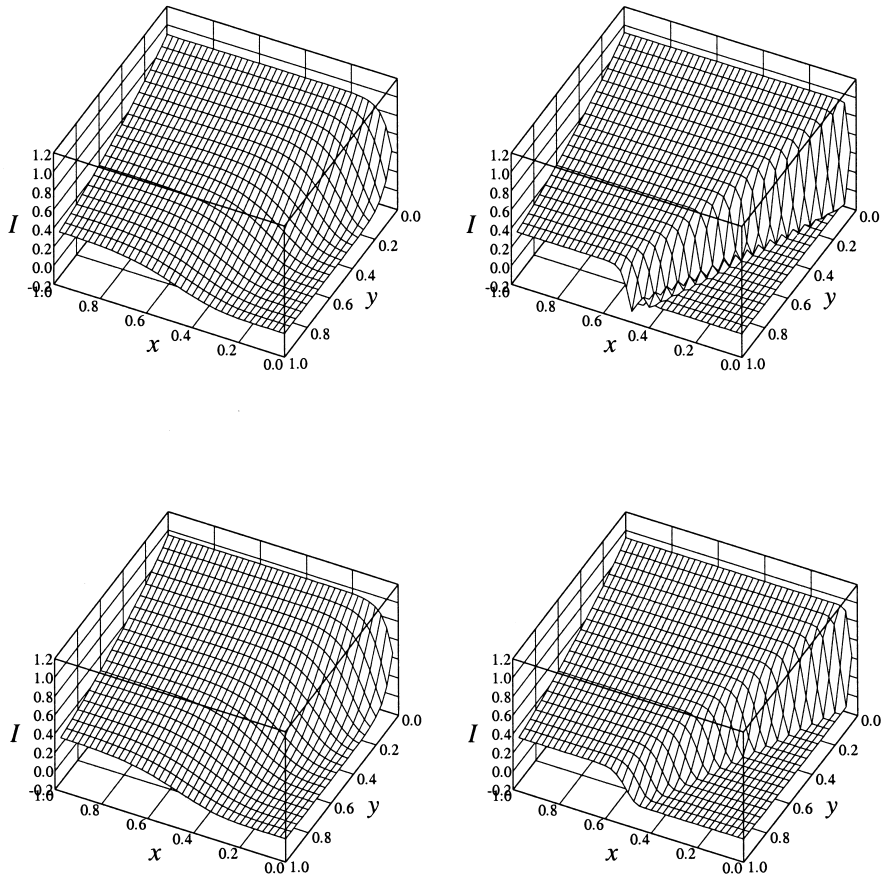

(a) step scheme (b) positive scheme

(c) modified-exponential scheme (d) hybrid scheme

Fig. 7. Intensity distribution for purely absorbing medium in an arbitrary direction ($\mu_m = 0.47925$, $\xi_m = 0.87768$).

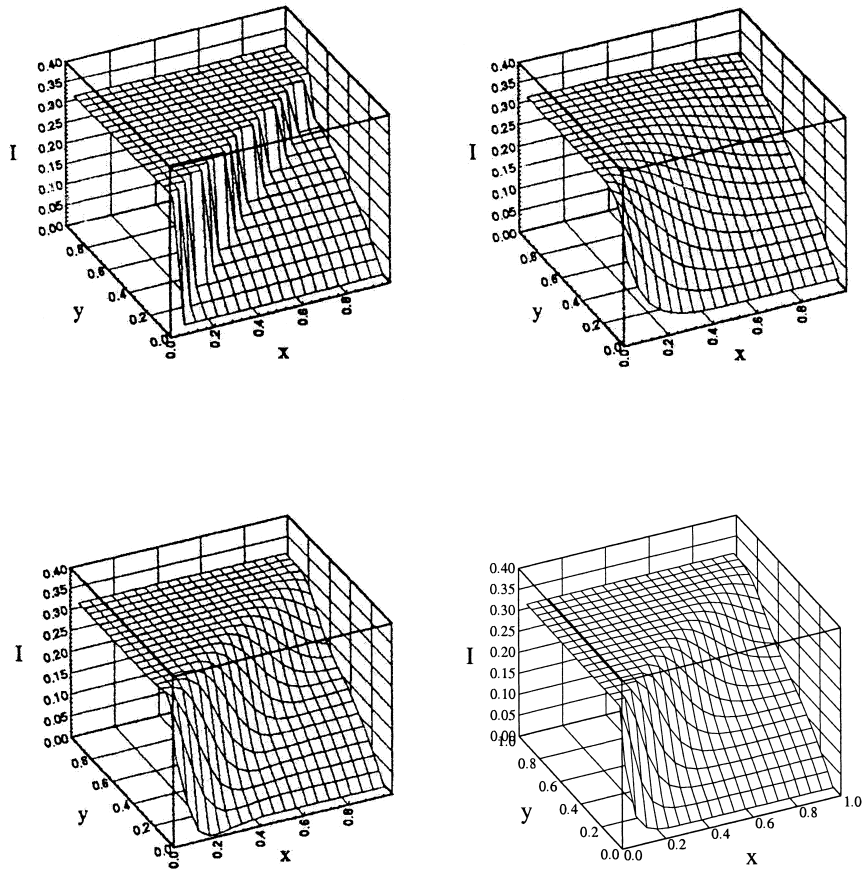

Fig. 8. Intensity distribution for absorbing-emitting medium in an arbitrary direction ($\mu_m = 0.8040087$, $\xi_m = 5773503$).

as M increases. This phenomenon results from the ray effect that causes radiation intensity not to continuously arrive at the wall due to discrete ordinates. For $M = 50$, the ray effect disappears and the result is the same as the one from Radiosity/Irradiation Method (RIM). For $M = 15$ and 25, local heat flux near $\zeta = 2$ (the upper right-hand corner) shows some deviation from one of the RIM because the ray effect is clearly seen at the diagonal direction, where there is no numerical smearing. Numerical smearing does not occur in this case because when M is odd (15, 25), the ordinate direction coincides with the diagonal direction of the grid. On the contrary, when M is even, the deviation of the heat flux disappears due to the even distribution of numerical smearing to all directions.

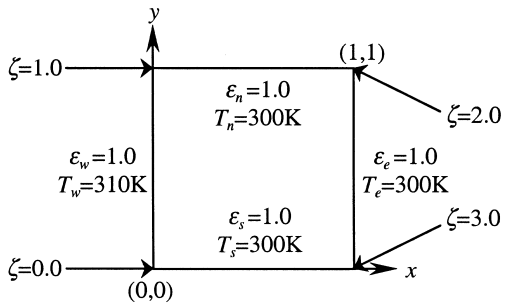

Fig. 9. Schematic diagram of a rectangular enclosure.

Overall heat fluxes and view factors on the north and east walls for 20×20 and 60×60 grid systems are

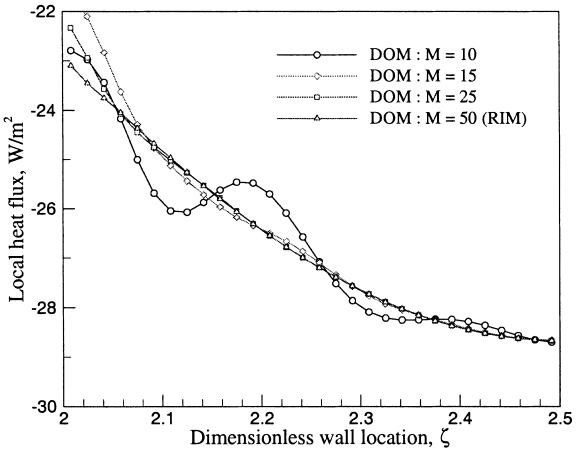

Fig. 10. Local heat fluxes at the east wall for the rectangular enclosure.

presented in Table 1. The view factors are enclosed within curly brackets and the results for the 60×60 grid are enclosed within parentheses. It is shown that the results from the step scheme, modified-exponential scheme, and variable-weight scheme of Sanchez and Smith [17] deviate further from those of the RIM as M increases. This means that the amount of numerical smearing increases as the number of ordinates increases. But the positive and hybrid schemes predict the same results in a non-participating medium ($\beta = 0$) with a square grid ($\Delta x = \Delta y$). The results from both schemes are closer to those of the RIM than other schemes because these two schemes produce less numerical smearing than the others do. When M is even, both of them predict the exact solution, and it is observed, especially for $M = 10$, that the effect of oscillation of local heat flux (Fig. 10) is countervailed due to averaging over the wall. However, these two schemes produce results different from RIM with odd values of M, since there exists a direction where ray effect is very significant.

4.2. Purely absorbing medium

The physical situation considered in this case is a square enclosure with purely absorbing medium ($\kappa L_x = \kappa L_y = 1$) and only the bottom wall ($y = 0$) is kept hot ($I_b = 1$). S-10 ordinates set and a 59×59 grid system were used for analysis. Average incident radiation at four locations is presented in Table 2 to examine the accuracy of each spatial differencing scheme.

The modified-exponential scheme used the results from the step scheme to avoid divergence in the initial computation since it includes a source term, S^m, in Eq. (21).

Table 2 shows that most of the spatial differencing schemes predict the results closer to those of Pessoa-Filho and Thynell [9] except at the center of the enclosure, $(0.5L_x, 0.5L_y)$. It seems that this results from the difference between DOM and the analytical method of Pessoa-Filho and Thynell [9]. It is also shown in Table 2 that the positive and hybrid schemes predict the results more accurately over the other schemes. However, the positive scheme needs the fix-up procedure since it may produce negative intensity when a non-uniform grid clustered to the wall is used to exam-

Table 1
Overall heat fluxes[a]

DOM (M)	Heat flux		
	Step, modified-exponential	Variable-weight [17]	Positive, hybrid
		North wall	
10	−18.351 (−18.709)	−18.790 (−18.844)	−18.849 (−18.849) {0.292893}
15	−18.324 (−18.683)	−18.764 (−18.834)	−18.912 (−18.912) {0.293862}
20	−18.315 (−18.674)	−18.755 (−18.824)	−18.849 (−18.849) {0.292893}
25	−18.311 (−18.670)	−18.751 (−18.820)	−18.872 (−18.872) {0.293242}
50	−18.305 (−18.664)	−18.745 (−18.814)	−18.849 (−18.849) {0.292893}
RIM	−18.849		{0.292893}
		East wall	
10	−27.654 (−26.937)	−26.775 (−26.667)	−26.657 (−26.657) {0.414214}
15	−27.706 (−26.989)	−26.827 (−26.687)	−26.532 (−26.532) {0.412275}
20	−27.725 (−27.007)	−26.846 (−26.708)	−26.657 (−26.657) {0.414214}
25	−27.733 (−27.016)	−26.854 (−26.716)	−26.612 (−26.612) {0.413516}
50	−27.744 (−27.027)	−26.865 (−26.727)	−26.657 (−26.657) {0.414214}
RIM	−26.657		{0.414214}

[a] 20×20 grid, (60×60 grid), {view factor}.

Table 2
Incident radiation predicted by various spatial differencing schemes in the case of purely absorbing medium[a]

Position	Grid	$G/4\pi$				
		Spatial differencing schemes				
		Step	Positive	Modified-exponential	Hybrid	Pessoa-Filho and Thynell [9]
$(0.5L_x, 0.5L_y)$	UG	0.11740	0.11632	0.11807	0.11607	0.11753
	NG	0.11684	–	0.11940	0.11648	
$(0.5L_x, L_y)$	UG	0.04107	0.03825	0.04041	0.03866	0.03863
	NG	0.04234	–	0.04115	0.03954	
$(0, 0.5L_y)$	UG	0.07445	0.07550	0.07336	0.07537	0.07525
	NG	0.07343	–	0.07215	0.07504	
$(0, L_y)$	UG	0.03055	0.02979	0.02933	0.02997	0.02986
	NG	0.03083	–	0.02993	0.02984	

[a] UG — uniform grid; NG — non-uniform grid.

ine the effect of grid. It is also evident from Table 2 that the hybrid scheme predicts more accurate results than the step and modified-exponential schemes even in the case of a non-uniform grid.

4.3. Purely scattering medium

For the purely scattering medium ($\sigma_s L_x = \sigma_s L_y = 1$) in the same enclosure considered in the previous case, Fig. 11 shows the comparison of the distributions of average incident radiation ($G/4\pi$) at $x/L_x = 0.1, 0.3$, and 0.5 between the results of the hybrid scheme and Thynell and Ozisik [19].

It is shown in Fig. 11 that the results of the hybrid scheme with S-10 ordinates set agree well with those of Thynell and Ozisik [19], except at $x/L_x = 0.5$ where there exists a little disagreement between the two results. It is believed that this disagreement is attributed to the ray effect.

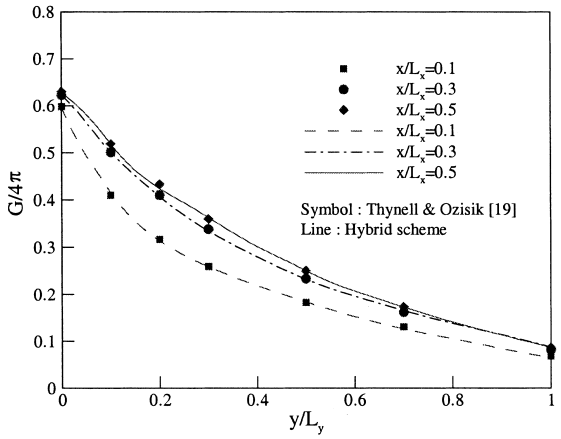

Fig. 11. Incident radiation for purely isotropically scattering medium.

Presented in Table 3 is the average incident radiation at four locations in the enclosure to examine the accuracy of the results from the various spatial differencing schemes in the case of a purely scattering medium.

Table 3 shows that in the case of uniform grid, the results from the positive and hybrid schemes are closer to those of Thynell and Ozisik [19]. However, in the case of a non-uniform grid, the positive scheme needs the fix-up procedure as in the case of the purely absorbing medium.

4.4. Absorbing–emitting–isotropically scattering medium

For the absorbing–emitting–isotropically scattering medium ($\kappa L_x = \kappa L_y = \sigma_s L_x = \sigma_s L_y = 0.5$) the average incident radiations at four locations are presented in Table 4.

It is also shown that the hybrid scheme yields more accurate results than the other schemes in both uniform and non-uniform grids, similar to the results of previous two media.

4.5. Consideration of exponential function in the hybrid spatial differencing scheme

In fact, the use of exponential function is expensive to evaluate. Hence, the application of Taylor series expansion to the exponential function may be helpful. The maximum errors between truncated and original forms of exponential function are presented in Table 5 when only the first two terms in Taylor series expansion are used in the case of a purely scattering medium.

It is shown that the maximum error of weighting factor is 36.237% when $\beta = 10$. However, the maxi-

Table 3
Incident radiation predicted by various spatial differencing schemes in the case of purely scattering medium[a]

Position	Grid	$G/4\pi$ spatial differencing schemes				
		Step	Positive	Modified-exponential	Hybrid	Thynell and Ozisik [19]
$(0.5L_x, 0.5L_y)$	UG	0.25000	0.25000	0.25000	0.25000	0.250
	NG	0.25000	–	0.25000	0.25008	
$(0.5L_x, L_y)$	UG	0.08933	0.08612	0.08951	0.08657	0.086
	NG	0.09193	–	0.09091	0.08770	
$(0, 0.5L_y)$	UG	0.14128	0.14231	0.14069	0.14210	0.142
	NG	0.13999	–	0.13942	0.14151	
$(0, L_y)$	UG	0.05935	0.05878	0.05870	0.05887	0.059
	NG	0.05990	–	0.05898	0.05887	

[a] UG — uniform grid; NG — non-uniform grid.

mum error of incident radiation for this case is only 0.8%. Hence, it indicates that truncated forms of the exponential function can be used without any significant error.

5. Conclusion

Since the hybrid scheme proposed in the present study incorporates the strengths from the diamond and step schemes, and takes into consideration the characteristics of the medium, it shows less numerical smearing than the step scheme, and it does not have the under-/over-shooting like the diamond scheme. The hybrid scheme also does not need to iteratively modify the spatial differencing weight as in the variable-weight scheme, and its numerical procedure is much simpler than other higher-order type schemes.

By applying the present hybrid scheme to 2D rectangular enclosures with non-participating, purely absorbing, purely scattering, and absorbing–emitting–isotropically scattering media, the following conclusions are obtained:

1. Hybrid scheme yields the results closer to the exact solution since it includes less numerical smearing than other schemes such as step, diamond, positive, and modified-exponential schemes.
2. Hybrid scheme does not need the fix-up procedure since it predicts physically realistic results, irrespective of the ordinates set and medium.
3. It is shown that hybrid scheme using the ordinates set with equal weights and equal angular increment predicts more accurate results. It is desirable for the hybrid scheme to use the ordinates set with equal angular increment to reduce the imbalance of the amount of numerical smearing, since the hybrid scheme has little numerical smearing along the diag-

Table 4
Incident radiation predicted by various spatial differencing schemes in the case of absorbing–emitting–isotropically scattering medium[a]

Position	Grid	$G/4\pi$ spatial differencing schemes				
		Step	Positive	Modified-exponential	Hybrid	Thynell and Ozisik [19]
$(0.5L_x, 0.5L_y)$	UG	0.16290	0.16224	0.16368	0.16234	0.1631
	NG	0.16242	–	0.16474	0.16225	
$(0.5L_x, L_y)$	UG	0.05719	0.05399	0.05668	0.05444	0.0542
	NG	0.05872	–	0.05769	0.05539	
$(0, 0.5L_y)$	UG	0.09782	0.09891	0.09705	0.09875	0.0988
	NG	0.09666	–	0.09581	0.09830	
$(0, L_y)$	UG	0.04026	0.03957	0.03927	0.03981	0.0396
	NG	0.04063	–	0.03978	0.03961	

[a] UG — uniform grid; NG — non-uniform grid.

Table 5
Maximum error between truncated and original forms of exponential function[a]

β		Maximum error of weighting factor (%)	Maximum error of results (%)
1.0	UG	0.063	0.0005
	NG	0.274	0.002
5.0	UG	1.643	0.05
	NG	7.675	0.1
10.0	UG	7.090	0.5
	NG	36.237	0.8

[a] UG — uniform grid; NG — non-uniform grid.

onal direction of the grid, but it shows numerical smearing in other directions of the grid.

4. The hybrid scheme predicts stable results even with a non-uniform grid and seems to be more superior to other schemes. This characteristic suggests that the hybrid scheme proposed in this study can be applicable to the combined heat transfer problem, including radiative heat transfer in the fluid flow and thermal analysis.

References

[1] S. Chandrasekhar, Radiative Transfer, Dover, New York, 1960.
[2] B.G. Carlson, K.D. Lathrop, in: H. Greenspan, C.N. Kelber, D. Okrent (Eds.), Transport Theory — The Method of Discrete Ordinates, Computing Methods in Reactor Physics, Gordon and Breach, New York, 1968.
[3] W.A. Fiveland, Discrete-ordinates solutions of the radiative transport equation for rectangular enclosures, ASME Journal of Heat Transfer 106 (1984) 699–706.
[4] S.V. Patankar, Numerical Heat Transfer and Fluid Flow, McGraw-Hill, New York, 1980.
[5] J.C. Chai, H.S. Lee, S.V. Patankar, Ray effect and false scattering in the discrete ordinates method, Num. Heat Transfer Part B 24 (1993) 373–389.
[6] J.P. Jessee, W.A. Fiveland, Bounded, high-resolution differencing schemes applied to the discrete ordinates method, Journal of Thermophysics and Heat Transfer 11 (1997) 540–548.
[7] G.D. Raithby, E.H. Chui, A finite-volume method for predicting a radiant heat transfer in enclosures with participating media, ASME Journal of Heat Transfer 112 (1990) 415–423.
[8] M.Y. Kim, S.W. Baek, Radiation in axisymmetric cylindrical coordinates with the modified discrete-ordinates method, Journal of the Korean Society of Mechanical Engineers (B) 22 (1998) 213–220 (in Korean).
[9] J.B. Pessoa-Filho, S.T. Thynell, An approximate solution to radiative transfer in two-dimensional rectangular enclosures, ASME Journal of Heat Transfer 119 (1997) 738–745.
[10] A.A. Mohamad, Local analytical discrete ordinate method for the solution of the radiative transfer equation, Int. J. Heat Mass Transfer 39 (1996) 1859–1864.
[11] K.B. Cheong, T.H. Song, Examination of solution methods for the second-order discrete ordinate formulation, Num. Heat Transfer Part B 27 (1995) 155–173.
[12] J.C. Chai, H.S. Lee, S.V. Patankar, Evaluation of spatial differencing practices for the discrete-ordinates method, Journal of Thermophysics and Heat Transfer 8 (1994) 140–144.
[13] K.D. Lathrop, Spatial differencing of the transport equation: positivity vs. accuracy, Journal of Computational Physics 4 (1969) 475–478.
[14] T.K. Kim, H.O. Lee, Effect of anisotropic scattering on radiative heat transfer in two-dimensional rectangular enclosures, Int. J. Heat Mass Transfer 31 (1988) 1711–1721.
[15] K.D. Lathrop, B.G. Carlson, Numerical solution of the Boltzmann transport equation, Journal of Computational Physics 2 (1967) 173–197.
[16] A.S. Jamaluddin, P.J. Smith, Predicting radiative transfer in rectangular enclosures using the discrete ordinates method, Combustion and Technology 59 (1988) 321–340.
[17] A. Sanchez, T.F. Smith, Surface radiation exchange for two-dimensional rectangular enclosures using the discrete-ordinates method, ASME Journal of Heat Transfer 114 (1992) 465–472.
[18] J.C. Chai, H.S. Lee, S.V. Patankar, Finite volume method for radiation heat transfer, Journal of Thermophysics and Heat Transfer 8 (1994) 419–425.
[19] S.T. Thynell, M.N. Ozisik, Radiation transfer in isotropically scattering rectangular enclosures, Journal of Thermophysics and Heat Transfer 1 (1987) 69–76.